COSMIC RAY AND RADIATION BELT HAZARDS FOR SPACE MISSIONS

M.I. PANASYUK
Skobeltsyn Institute of Nuclear Physics, Moscow State University, 119899 Moscow, Russia.

Key words: radiation belts, galactic cosmic rays, solar energetic particles

Abstract

The main components of the radiation environment, surrounding the Earth are: galactic cosmic rays, solar energetic particles and the radiation belts. All these components are subject to studies from the point of view of radiation impact on biological structures and spacecraft elements. Galactic cosmic rays which mainly consist of protons and nuclei and especially their highly ionizing component (heavy nuclei) are the predominant source of radiation damages in condensed matter at micro-volume level, causing such malfunctions in electronic devices such as latch-ups, single event upsets and ets. Energetic particles generated in solar flares and coronal mass ejections can also lead to serious radiation hazards. During periods of powerful solar events, lasting several days and accompanied by magnetic storms, the most highly energetic solar particles can overcome the barrier, induced by the magnetic field, reaching low altitudes. In this case, the radiation doses from solar particles can significantly exceed the corresponding doses from trapped particles.

The solar energetic particles exhibit a long-term variation associated with the 11-year solar activity cycle. The physical interpretation and model representation of this variation is far from being complete. The fluxes of particles in the radiation belts are the highly dynamical .Temporal variations of the particle fluxes (mainly electrons and protons) undergo intensity variations on time scales from about 1 minute to several years. Rapid variations, generally, are associated, with the generation of electric fields and electromagnetic emissions during substorm activity, while slow variations are induced by variations of solar activity and, as a consequence, by variations of particle transport velocities and loss rates inside the radiation belts. No comprehensive engineering model of the radiation belts that would adequately describe their spatial and dynamic properties is yet available.

Radiation hazard for space vehicles in near-Earth space is caused by a number of factors among which, besides the time of exposure to the radiation environment, the most significant are the orbital parameters of satellites, as well as the levels of solar and geomagnetic activities leading to radiation flux enhancement.

1. Introduction

The high-energy electrons, positrons, protons, nuclei and ions of different elements, encountered in space (with energies from hundreds keV to tens GeV), are one of the most important projectiles affecting spacecraft operation and constituting hazard for living organisms onboard any spaceship. This is due to the ability of these particles to penetrate the shielding material and to their interactions with spacecraft elements, electronics, and biological structures (i.e. any matter in condensed state).

The radiation environment of interplanetary space is composed of particle fluxes of solar and galactic origin. Solar activity is the most critical factor, determining their characteristics (flux dynamics and energy spectra).

The radiation environment in the vicinity of the Earth, surrounded by a magnetic field, contains a larger number of different components, than the radiation in the interplanetary medium. Among them are the radiation belts (RB), a stable formation, trapped by the Earth's magnetic field, it contains radiation of both solar and terrestrial origin. The RB environment is determined by the albedo of secondary particles, which are the result of cosmic ray interactions with the atmosphere, as well as particles, precipitated from the radiation belts. The main factor, that influences the dynamics of the spatial distribution of the RB, are geomagnetic disturbances (storms and substorms), which as a rule, occur during solar wind plasma interactions with the interplanetary and the Earth's magnetic fields. The other components of the energetic particles in near-Earth space are galactic cosmic ray (GCR) and solar energetic particles (SEP), penetrating into the geomagnetic field.

The numerous components of the radiation environment, with their different physical characteristics, and various mechanisms of their interaction with matter, complicate modeling of the environment and predictions of their impact on objects flown in space.
This paper presents a survey of our current understanding of the basic components of the surrounding radiation environment, and the mechanisms of their impact on matter. The empirical models, used to evaluate the radiation effects are also discussed.

2. Space Radiation - a Short Overview

2.1. THE EARTH'S RADIATION BELTS

The radiation belts are fluxes of energetic particles, confined inside the geomagnetic trap, located in the Earth's inner magnetosphere at equatorial distances ranging from 1.2 to 7 R_e (Earth radii). The RB predominantly consist of electrons and protons, however, heavy ions (at least up to Fe) are also present. The typical energies for ions are from ~100 KeV/nucleon to several MeV/nucleon, and for electrons from ~100 KeV to several MeV. The low energy boundary is somewhat conventional and corresponds to the highest energy of hot ring current plasma (tens keV/nucl) inside the magnetosphere, whereas, the upper boundary is determined by the value of the adiabaticity parameter (see for example (Morfill, 1973 and Ilyin et al., 1988)) $\kappa = \rho_L / \rho_m$, where ρ_L is the Larmor radius, and ρ_m is the curvature radius of the magnetic field line. The value of $\kappa \approx 0.1$ defines the maximum energy of electrons and ions for stable trapping on a given L-shell.

The charge state of trapped ions depends on their sources and charge-exchange with the background neutral exosphere.

The RB space-energy distribution (Fig.1) is different for electrons and protons: the electrons form an inner and outer belt, whereas the protons display a continuous increase of mean particle energy with increasing L-shell value. The most energetic protons populate the inner zone at L<2.5. Particle energy increase due to betatron acceleration occurs during their propagation across the *L*-shells (radial diffusion) caused by fluctuations of the magnetic field and/or electric fields in the magnetosphere (see, e.g. (Tverskoy, 1964 and Spjeldvik, 1977)). The gap between the inner and outer radiation belts results from particle scattering by electromagnetic waves.

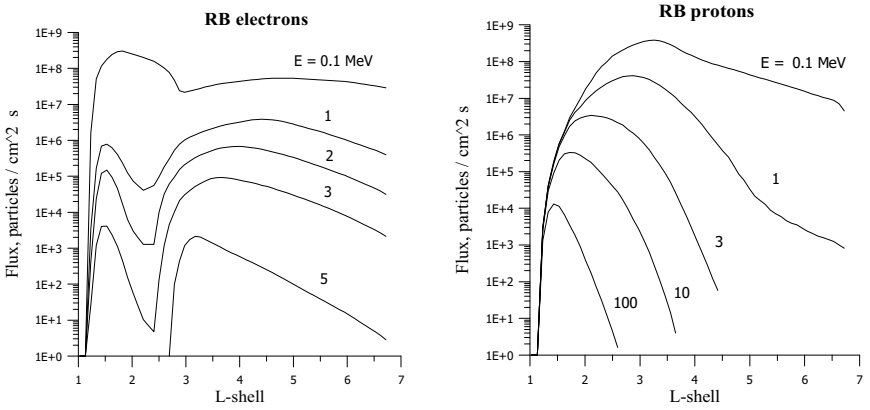

Fig.1. Radial profiles of radiation belt proton and electron intensities in the geomagnetic equator plane.

The main sources of RB particles are the solar wind, the ionosphere, and secondary (albedo) particles (see 2.5), which are produced as a result of cosmic ray interactions with the atmosphere. Each of these sources contributes to the population of radiation belt particle population. Hence, the atmospheric source, unlike the solar one, mostly contributes singly-charged heavy ions (He^{+}, O^{+}) to the inner magnetosphere. Solar ions are typically multiply-charged heavy ions (He^{2+}, O^{6+}, Fe^{12+}).

Both these sources are responsible for populating the outer zone of the RB. The inner zone sources are mostly albedo particles - the result of GCR interactions with the atmosphere.

2.2. GALACTIC COSMIC RAYS

GCR are fully ionized particles of all existing elements with relativistic energies (ranging from ~10^{8} eV to at least ~10^{21} eV). Their chemical composition approximately corresponds to the mean element abundance in the Universe (90% of protons, ~7% helium nuclei, etc.) GCR are of galactic and extra-galactic origin. At energies below 10^{15} eV their origin is associated with supernova blasts, at larger energies their origin is still unclear (see, for example, the survey (Gloeckler, 1979). Inside the heliosphere the energy spectrum of GCR has a distinct maximum (Fig. 2) at energies of 0.3-1

GeV/nucleon. It is caused by modulation of GCR fluxes at energies below the maximum by the variable interplanetary magnetic field, which depends on the cycle of solar activity. The typical period of this modulation is about 11 years, however, periods with other duration have been identified.

The penetration of particles inside the geomagnetic field is determined by its magnetic rigidity:

$$R = \frac{A}{Q}\sqrt{E(E+2Mc^2)} \quad (1)$$

where A is the mass number, Q is the charge, and M is the mass of the charged particle with energy E. The GCR radiation flux inside the magnetosphere changes due to the 'geomagnetic cut-off effect' which is determined by the deflection angle of a particle inside the geomagnetic field from its incident or initial direction. Hence, the energy spectrum of GCR is distorted due to the filtering effect of the geomagnetic field. GCR flux characteristics inside the magnetosphere are determined by the distortions of the Earth's magnetic field during its interactions with coronal ejections of solar plasma, as well as magnetic storms and substorms, associated with plasma injections into the inner magnetosphere.

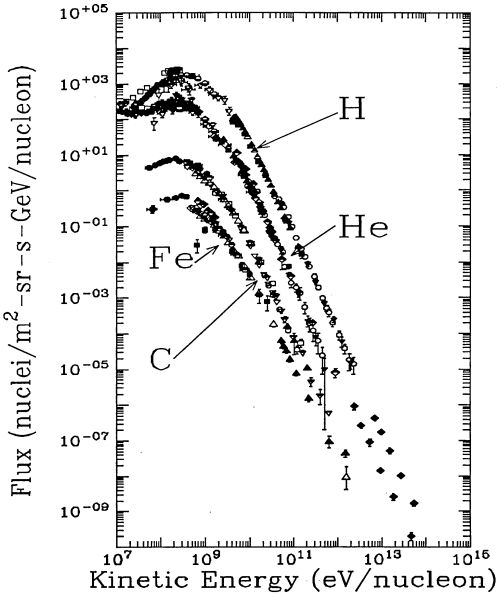

Fig.2. The energy spectrum of galactic cosmic ray nuclei (Ormes, Betty, et al., 1994)

2.3. THE ANOMALOUS COSMIC RAY COMPONENT

The anomalous component of cosmic rays (ACR) is the least energetic part of GCR their mean energies are of tens MeV (see Fig. 3). They mostly consists of O, N, Ne, Ar and Si ions. Unlike the regular GCR component, the

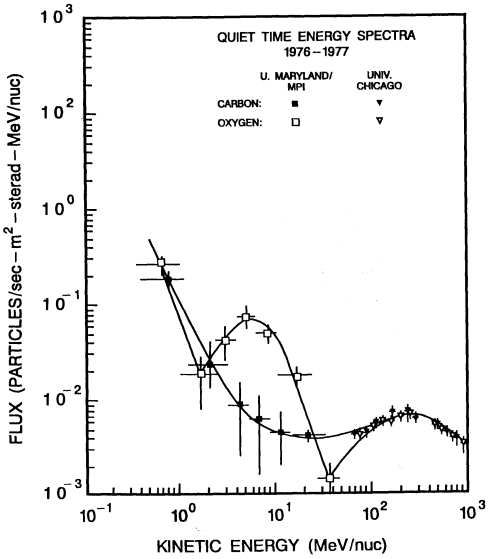

Fig.3. The energy spectrum of anomalous cosmic ray oxygen and carbon nuclei (Gloeckler, 1979).

predominant charge state of ACR ions is 1+, 2+ (see, e.g. (Blake and Friesen, 1977 and Panasyuk, 1993)). Like GCR, ACR fluxes experience an 11-year solar modulation cycle. ACR with the lowest charge states, penetrate deepest inside the Earth's magnetic field, where they interact with the atmosphere, undergoing charge-exchange. Part of these stripped ions, with higher charge states (upto +8 for oxygen), become stable trapped and form an ACR radiation belt (see, e.g. (Grigorov et al., 1991)).

2.4. SOLAR ENERGETIC PARTICLES

These particles are generated in solar flares and coronal mass ejections (CME). The maximum energy of these particles is ~ 100 MeV/nucleon. However sometimes, during gigantic solar events, their energies reach ~ GeV/nucleon. The ionization states of SEP can range from fully ionized for the light ions (protons, He) to partially ionized for heavier atoms (Fe), depending on the solar coronal temperature and the SEP propagation through the interplanetary medium.

SEP occurrence frequency depends on solar activity, displaying a tendency for greater occurrence frequency during maximum solar activity and during decline of the cycle. The chemical composition of SEP varies around the mean elemental composition of the Sun: protons being always predominant, He ions constitute several percent and heavier elements are much less abundant. The measured fluence of SEP events varies within a wide range from 10^5 to 10^{11} particles/cm^2 . The duration of the event can range from one to several days. In comparison to GCR, SEP particle spectra are softer, and therefore subject to greater distortion due to the geomagnetic cutoff when measured within the magnetosphere.

2.5. NATURAL ALBEDO RADIATION

Albedo radiation (AR) is the secondary radiation generated in the inner magnetosphere as a result of:
- nuclear reactions by cosmic ray (GCR, SEP) interactions with protons of the inner radiation belts and atoms of the atmosphere;
- secondary cosmic ray (muon) decay.

This radiation environment component mostly consists of:
- neutrons;
- gamma-quants;
- electrons and positrons;
- protons and nuclei.

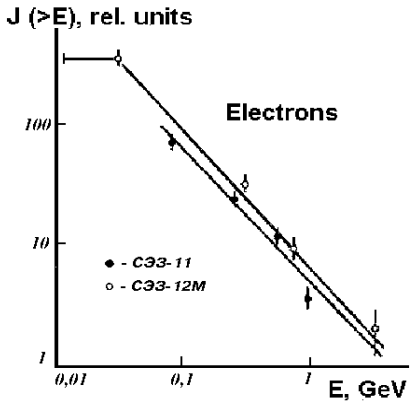

Fig.4. The energy spectrum of albedo electrons according to 'Proton 3 and 4' satellite data (Grigorov, 1985).

Fig.4 shows one of the first measurements of relativistic electrons, made in 1966-68 onboard the Proton 3, and 4 satellites at altitudes of ~ 350 km (Grigorov, 1985). The main result is an extremely hard spectrum ($\gamma \approx 1$) of secondary electrons, produced as a

result of $\pi-\mu-e$ decay. The integral flux of these albedo particles near the equator was equal to the flux of primary GCR particles.

Detailed data on albedo protons were recently obtained in the Alpha Magnetic Spectrometer experiment (AMS collaboration, 2000).

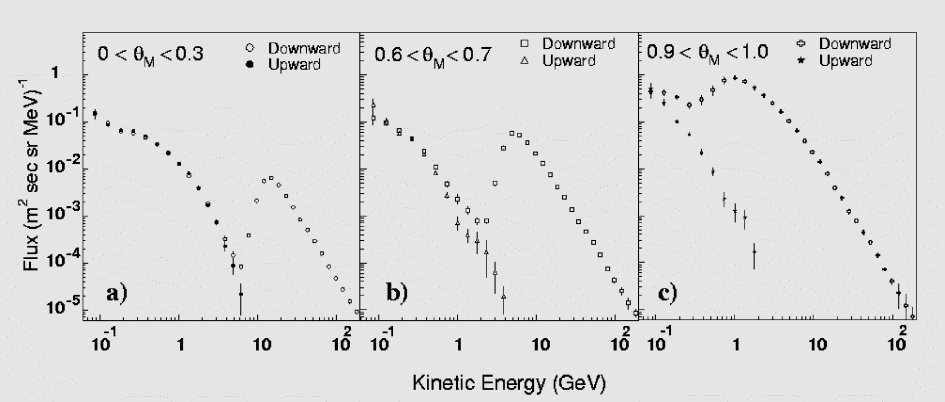

Fig.5. Comparison of upward and downward secondary spectrum of protons at different geomagnetic equatorial latitudes ϑ_m (in radians) (The AMS collaboration, 2000).

Fig.5 shows the energy spectra of albedo protons and protons originating in a restricted geographic region below the geomagnetic cutoff (the low energy part of the spectrum) and primary GCR at different latitudes (at ~400 km altitudes). It is obvious, that such secondary particles fluxes (the albedo radiation environment) should be accounted for in radiation impact models for low earth orbiting (LEO orbits) satellite.

3. The Main Radiation Effects in Energetic Particle Interactions with Matter

3.1. PARTICLE INTERACTIONS WITH MATTER

The mechanisms of particle losses depend on their energy. For example, the main losses for *ions* with 10^4-10^8 eV energies are ionization, i.e. the particle loses energy as it ionearizes and excites atoms of materials it traverses. For ions with energies exceeding 100 MeV/nucleon the major role is played by nuclear interactions. High energy *electrons* ($E_e >> m_o c^2$) lose energy mostly due to bremsstrahlung, whereas at energies $E_e << m_o c^2$ ionization losses are the most predominant loss mechanisms.

The mean free path, as well as linear energy loss per unit length (LET) in a given material, serves as a quantitative measure characteristic for interactions of penetrating radiation with matter. The electron component of radiation, has greater penetrating ability than the ion component. It is to a large extent responsible for the dose effects in matter. However, ions, especially heavy ones, cause larger energy release in a given volume in comparison to light ions and electrons and, therefore, can cause more significant local radiation damage in microvolumes of matter (high-integration electronics, biological structures at the cell level).

Photon and gamma-ray interactions with matter are also energy-dependent. At gamma-ray energies less than 1 MeV photo-effect is predominant. It leads to the production of low energy electrons, whereas at higher energies pair (electron-positron) production dominates. The Compton effect, accompanied by generation of electrons and gamma-ray scattering, dominates in the MeV energy range.

There are various types of *neutron* interactions with matter. They include elastic and inelastic scattering; radiation capture, accompanied by photon emission; capture, accompanied by charged particle emission and nuclear fission. The cross-sections of these processes depend on the neutron energy and differ for all atoms. Unlike photon interactions with matter, neutron interaction displays a resonance structure. In elastic interactions the neutron changes the direction of its velocity and loses part of its energy. Elastic scattering plays a major role in the attenuation of fast neutron fluxes (with energies from 0.2 to 20 MeV). The most efficient attenuation per unit mass is observed in media containing hydrogen. In this case the neutron energy decreases rapidly; the neutrons are thermalised (to energies from $5 \cdot 10^{-3}$ to 0.5 eV) and absorbed by hydrogen nuclei.

Inelastic scattering of neutrons has a threshold energy character and is most significant for heavy nuclei. If the energy of the incident neutron exceeds the energy of the first excited state of the target-nucleus, emission of one or several photons occurs, with a spectrum, typical of the nuclei. Neutron absorption belongs to the inelastic interaction type and for most elements occurs mainly in the thermal region of neutron energies. The trapping cross-section in this case is proportional to $1/\sqrt{E}$. Photon emission occurring in radiation trapping has sufficiently high energy (6-8 MeV) and plays an important role in the formation of radiation fields behind shielding. Inelastic interactions of neutrons also include reactions involving charged particle production: (n,p), (n,α), etc.

As we will see below, besides single event upsets in mirochips, the neutron component of space radiation (mainly of albedo and local origin) contributes a major dose in thick shields.

3.2. RADIATION EFFECTS CAUSED BY IONIZATION IN SOLID BODIES

Numerous types of radiation transformations occur in particle interactions with solid bodies (Fig. 6). Such interactions can be both reversible and irreversible. The main types of radiation transformation can conventionally be separated into three groups - ionization effects, charge transfer effects, and displacement effects. A detailed review can be found in the paper by Vampola (1994).

3.2.1. *Ionization Effects*

The electron-hole pairs generated as a result of ionization energy losses lead to new reversible and irreversible properties in materials, such as radiation conductivity, radiation coloring, radioluminescence, radiation-chemical effects, etc. Radiation conductivity and radioluminescence are mainly determined by the dose rate and are reversible; they rapidly (< 1 mcs) disappear when irradiation stops. Radiation-chemical

transformations, and radiation coloring, on the contrary, depend on the absorbed dose, and the relaxation time for these effects can be quite long - from 1 to 10^7 seconds and even longer.

3.2.2. *Charge Transfer Effects*

Compton currents arising under the impact of high-energy gamma-rays, or proton recoil during bombardment of light matter by neutrons, are typical examples of charge transfer effects. As a result of radiation impact electric charges can be induced inside the dielectric. The magnitude of this charge density depends on the radiation dose.

3.2.3. *Displacement Effects*

These effects are associated with displacement of the atoms in a solid body from the crystalline lattice nodes due to energy losses of the interacting particles. The critical energy for the displacement effects depends on the bombarded atoms in the crystal and on the nature of the incident particles: thus, in silicon it is 106 eV for protons and 160 keV for electrons. Displacement effects in a solid body lead to long and short-time defects. As a rule, irradiation by relativistic electrons and gamma-rays (~ 1 MeV), causes simple primary defects. Irradiation by neutrons, protons, and electrons of higher energies is usually accompanied by a cascade of defects.

3.3. RADIATION DAMAGE IN MATERIALS AND SYSTEMS

Radiation stability of materials and systems/components is their ability to operate and preserve initial characteristics under the impact of radiation. Radiation impact causes two types of effects in the satellite's components and materials: gradual degradation of operating abilities due to absorbed dose accumulation and upsets in microelectronics caused by single ion penetration. We will now consider some aspects of both effects.

3.3.1. *Dose Effects*

Numerous results of laboratory testing and operation of satellite experiments provided data on the radiation stability of satellite materials and components (Akishin et al., 1983). Some of these data are reported in Table 1.

One of the most well studied examples of radiation damage in satellite systems is solar panel degradation. The main reason of their degradation is the decrease of the life-times of minority carriers in the semiconductor base region due to radiation defects. Under the impact of ionizing radiation the following relation is valid:

$$1/t = 1/t_0 + k/F \qquad (2)$$

TABLE 1. Radiation stability characteristics for some satellite materials and components.

Material, or system	Irradiation dose, Gr	Impact characteristics
Semiconductor instruments	10^3-10^4	Backward current increase, amplification decrease
Solar panels	10^3-10^4	efficiency decrease
Optical mirrors	10^3-10^4	Transparency degradation
Fiber optics	10^2-10^3	transmitted signal damping
Polymer materials	10^4-10^6	Degradation of mechanical and insulating properties
Thermal-insulation coatings	10^5-10^7	Increase of solar radiation absorption coefficient
Metals	10^9-10^{10}	Degradation of metallic properties

Where t_0, t are the carrier life times, before and after irradiation by fluence F, and k is the damage coefficient (which is different for electrons and protons). For typical energies of electrons (0.5-4 MeV) and protons (30 MeV), responsible for radiation damage in solar panels, the value of k is equal to ~10^{-9} and 10^{-6} respectively. A large decrease of solar panel operation efficiency is necessarily expected in the inner zone of the radiation belts, where the high energy proton fluxes are largest (see Fig.1.)

Fig.7 shows variations of silicon solar panel characteristics measured on the 'Electron-3' satellite. The use of transparent glass shielding permitted to improve the radiation stability of the silicon solar panels during the mission.

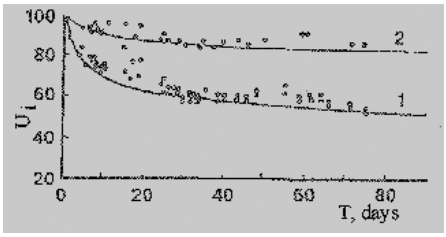

Fig.7. Relative idle run voltage decrease in silicon solar panels on the 'Electron-3' satellite. 1- without shielding, 2 - with glass shielding (Akishin et al, 1983)

Radiation impact on systems onboard satellites can lead to fatal consequences. A dramatic case of solar panel degradation is known for two satellites Transit 4B and TRAAC after a nuclear explosion in space in 1962 (Ebert and Hoffman, 1999). The nuclear explosion produced additional radiation fluxes in the inner radiation belt zone, which sharply decreased the solar panel efficiency, and after a certain time period the onboard systems stopped working.

Another example of space radiation impact on the satellite components are electric discharges in the irradiated dielectrics. Dielectric materials irradiated by charged particles and gamma-rays can produce the accumulation of excessive charge densities. The interior electric charge creates a high electric potential difference. When the electric field intensity inside the irradiated dielectric volume induced by the implanted charge, exceeds the electric strength limit of a material (1-1.5 MV/cm) a breakthrough discharge of the dielectric to its surface will occur. Thus, a fluence of about 10^{12} particles/cm^2 is required to make a breakthrough in a Lihtenberg structure by 4 MeV

electrons. The charge inside the dielectric is determined by its structure, shape, interior resistivity, and the presence of capturing centers in the forbidden zones. Electric discharges in dielectrics under the impact of protons and electrons with energies of about 100 MeV, can generate a current pulse of 1-100 A with duration from 0.1 to 1 microsecond and current density up to 10^6 A/cm^2. Dielectric discharges and plasmoid relaxations cause electromagnetic emission in the 0.1-100 MHz frequency range. Such a wide scope of physical phenomena, accompanying electric discharge processes can, of course, lead to anomalies during satellite operation inside the radiation belts. Sporadic increases of relativistic electrons in the outer radiation belt zone have caused radiation anomalies in a number of instances (see, e.g. (Baker, 1996)).

3.3.2. Dose Effect Calculation Models

Primary particles and gamma-rays, as well as secondary particles, produced in primary particle interactions with satellite components, can penetrate within modules of the satellite. The absorbed dose is the universal measure of ionizing radiation impact on matter. It is defined as the amount of energy, absorbed by a unit mass of matter. Obviously, the dose load on any objects inside the spacecraft depends on the location of these objects, on the complexity of the satellite configuration and its non-uniform structure.

Radiation effect calculations are usually made in three steps:

1) Radiation environment determination, using corresponding empirical models. (see section 4).

2) Modeling of radiation penetration through shielding and calculations of the energy spectra of the particles, impacting the target. Here it is necessary to keep in mind the complexity of radiation propagation in a solid body. First of all, the stochastic range directions (especially significant for electrons), requires Monte-Carlo simulations. Secondly, particle propagation is accompanied by cascade processes and generation of secondary particles. The evaluation of these processes requires the use of complicated existing transport codes (like GEANT (CERN, 1994)). These transport codes provide inputs for the third stage of calculations.

3) Estimates of the total energy and/or the energy deposition rate in a target. At this stage it is important to simulate the geometry of the object. The accuracy of the final dose effect calculations depends on how well the geometrical model describes the actual object. The SHIELDOSE (Seltser, 1979) and RDOSE (Makletsov et al., 1997) models are sophisticated mathematical models currently used for calculations of the absorbed dose in complicated satellite systems.

3.3.3. *Single Event Upsets*

Radiation effects in on-board microprocessor systems onboard satellites were reported for the first time in (Binder et al., 1975). These effects are caused in most cases by single event upsets in digital integral microchips. SEU are associated with deceleration of high energy nuclei in the chip materials and accumulation of excess charges on their electrodes due to charge carrier separation in the ionization track of the nucleus. These nuclei, which are present both in the radiation belts and cosmic rays, penetrate directly

into the sensitive volume of the microchip and lead to upsets. The proton component can produce residual nuclei (in nuclear reactions) and nuclear recoil (in elastic collisions) which, in turn, initiate upsets. Another source of upsets are neutrons. They can form nuclei as a result of nuclear reactions in the material surrounding the microchip.

The predominant role of the heavy ions or the protons in upset occurrence depends on the relative fluxes of both components. The proton flux in GCR exceeds the heavy ion flux by 2-3 orders of magnitude, this prevents protons from being an efficient source of upsets, since the nuclear interaction probability for protons in chip materials is only $\sim 10^{-5}$-10^{-6}. The situation is different in the inner belt, where heavy ions are practically absent: here the upsets are mostly the result of electronic system irradiation by the proton component.

Besides single event upsets in microchips multiple upsets can occur for the following reasons:
- multiple penetration of a single ion through several chips;
- charge diffusion into several sensitive regions of the microchip;
- penetration of a cosmic ray induced shower.

SEU can be regarded as recoverable microchip failures. However, besides these effects, microchips can suffer single-particle radiation effects like dielectric layer breakdown, field transistor burn-through, etc., which lead to irrecoverable failures of the whole microchip or of one of its active elements.

3.3.4. Single Event Upset Effect Models

Numerous empirical and physical models have been developed for quantitative predictions of single event upset effects. (see e.g. (Pickel, 1996; Kuznetsov and Nymmik, 1994). There are models (mostly SEU occurrence models), that describe separately the impact of the ion and the proton radiation component. Models describing both these impacting mechanisms have also been developed.

The quantitative models are based on calculations of the critical charge (which leads to SEU effects). They take into account:
- the overall area and size of the microchip surface;
- the LET spectra of the interacting particles;
- mean free path distribution in the sensitive volume of the microchip. The numerical values of the model parameters for each microchip type are fitted to match the results of ground radiation testing.

4. Experimental and Model Characteristics of the Surrounding Radiation Environment

4.1. RADIATION BELTS

4.1.1. *Theoretical Model*

The spectral and spatial distribution of RB particles is mainly determined by their radial diffusion (see e.g. (Tverskoy, 1964 and Spjeldvik, 1977) which is driven by electric and magnetic field fluctuations. Radial diffusion is accompanied by particle transfer across the drift-shells. This process is described by the Fokker-Plank equation, which includes the transport term, and the terms responsible for particle losses.

The space-energy structure of the RB in scope of the diffusion equation is determined by the balance between particle transport across drift-shells and their losses (energy degradation, pitch-angle scattering, charge-exchange of ions). The particle radial transport inside the magnetosphere leads to particle energy increase with decreasing L-shell number, in concordance with betatron acceleration $E \propto L^{-3}$. The characteristic times of particle radial transfer are determined by the diffusion coefficients D and depend on the L-shell parameter. Thus, for diffusion driven by geomagnetic field fluctuations of the sudden commencement type (SC) (Tverskoy, 1964) the radial diffusion coefficient is approximated by the empirical formula:

$$D_m = D_{0m} L^{10} \qquad (3)$$

where D_{0m} depends on the frequency and amplitude (power spectrum) of the SC. The SC generates an induction electric field (E) which causes particles to across magnetic field lines. The SC are initiated by solar wind dynamic pressure and IMF variations. Therefore, significant correlation of long-period variations of D_m and the solar activity should be expected during the cycle of solar activity. As it can be seen from Fig.8, such a dependence be is actually observed.

The SC occurrence frequency dependence on the sunspot number W has a high positive correlation coefficient (0.87). Therefore, variations of D_m within the factor of 3-5 should be expected in the course of the solar activity cycle. On the other hand, particle (for example ion) losses are fully determined by the density of the atmosphere and the neutral exosphere, which also change during the solar activity cycle (displaying the opposite dependence on W variations). These qualitative considerations of the physical radiation belt model indicates, that the use of empirical models, based on data sets corresponding to limited time intervals can hardly be justified for engineering calculations regarding other time intervals.

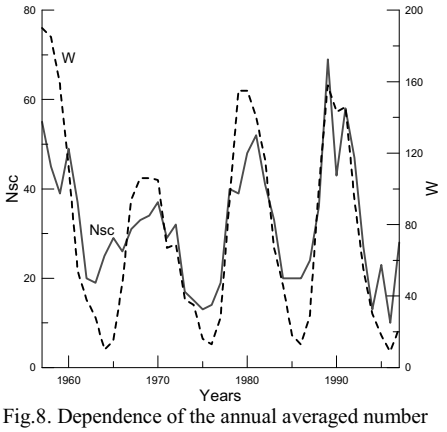

Fig.8. Dependence of the annual averaged number of storm sudden commencements (N_{sc}) on sunspot number W (Kuznetsov et al., 1999).

4.1.2. *Empirical Models*

The most extensively used empirical models of the RB are AE-8 and AP-8, for the electron and proton trapped radiation components, respectively (Vette, 1991; Sawyer

and Vette, 1979). These models are based on averaged experimental data mainly obtained during the epoch of 1960-1970 (a time interval from solar activity decline to solar activity maximum). This means the use of transport parameters for the physical model, averaged over the whole interval of this solar minimum period. In other words, the AE-8 and AP-8 models (as well as similar Skobeltsyn Institute of Nuclear Physics (SINP) radiation belt model – RB/SINP (GOST, 1986) represent the averaged space-energy distribution of the radiation belts, typical for certain phases of the solar activity cycle. A comparison between the NASA and SINP radiation belt models can be found in (Beliaev and Lemaire, 1994, and Beliaev and Lemaire, 1996). In this respect, calculations, based on these models, but made for other periods should be regarded only as indicative ones: i.e. as a first approximation of the actual values. More reliable estimates can only be obtained if additional experimental data are made available. Furthermore, the above mentioned models are essentially static, though they display the correct tendency of flux variations for solar cycle minimum and maximum periods.

The recently developed NOAAPRO (Huston et al., 1996), CRESSPRO and CRESSELE (Brautigam et al., 1992) models, can be regarded as dynamic, but they can only describe the proton and electron fluxes in the framework of the corresponding experiments: extrapolation of the calculations to other time periods is obviously controversial.

Therefore, there are several types of trapped radiation variations, that impair the accuracy of model calculation of radiation doses or other radiation effects based on these static empirical or statistical models .

4.1.3. *Variations of Trapped Radiation Fluxes*

The time variations The radiation belt space-energy distributions are numerous and have different physical origins. Basically all of these variations can be subdivided into main groups - adiabatic (i.e. occurring with conservation of the first, and the second adiabatic invariants) and non-adiabatic particle motion (i.e. non-conserving the adiabatic invariants). Adiabatic variations are slow compared to the gyroperiod the bounce period and the period of azimuthal drift. They correspond to slow variations of the surrounding magnetic and electric fields. In this case the space-energy distribution of the radiation belts is restored directly after the end of the disturbance.

Non-adiabatic variations can develop on different time scales. Several examples are presented and discussed in the famous (historical) paper by McIlwain (1996). Another classical example of non-adiabatic variations is the well known ‘transient’ event of May 24th, 1991, when RB electrons were accelerated up to ~15 MeV within minutes and protons up to ~40 MeV, at L~2.5 (Gussenhoven et al., 1992). On the other hand, there are secular variations of the Earth’s magnetic field, which lead to noticeable changes in the radiation fluxes in LEO on time scales of several decades. The trends on the distribution of RB particles resulting from these secular variations of the geomagnetic fields have been described and discussed in the final report of the TREND-2 study for ESTEC (Lemaire et al., 1995).

For the electron component it is necessary to mention the 27-day variations, associated with corotating solar wind fluxes (Williams, 1966), and seasonal variations, caused by changes of the geomagnetic dipole tilt angle relatively to the ecliptic plane

(Desorger, et al., 1998), as well as non-periodic variations. We will consider in more detail some of the variations and illustrate their effects on the electron and proton components.

Outer Belt Electrons. The most significant example of global variations of the outer zone electron component is radial transport of particles towards the Earth during geomagnetic disturbances (see, e.g. (Williams et al., 1968). During geomagnetic activity increases radial diffusion due to wave-particle interaction can be observed; the location of the outer radiation belt maxima (L_{max}) depends on the D_{st} variation amplitude: it is given by the empirical formula $L_{max} \propto |D_{st}|^{-4}$ (Tverskaya, 1996). Such waves diffusion are observed in a wide range of electron energies up to E>8 MeV (Vakulov, 1976). Long-term variations of L_{max} reflect to a larger extent variations of geomagnetic activity (D_{st}), than those of solar activity described by W, the sunspot number (Fig.9).

It is obvious that such types of variations should eventually be used in future dynamic models of the electron radiation belt component. A first electron model built along this line of thoughts has been proposed by D.J. Rodgers as part of the TREND-2 effort: his Kp - dependent electron model MEA3MSSL is based on the CRRES MEA observations for energies ranging between 153 and 1534 keV (Rodgers, 1996).

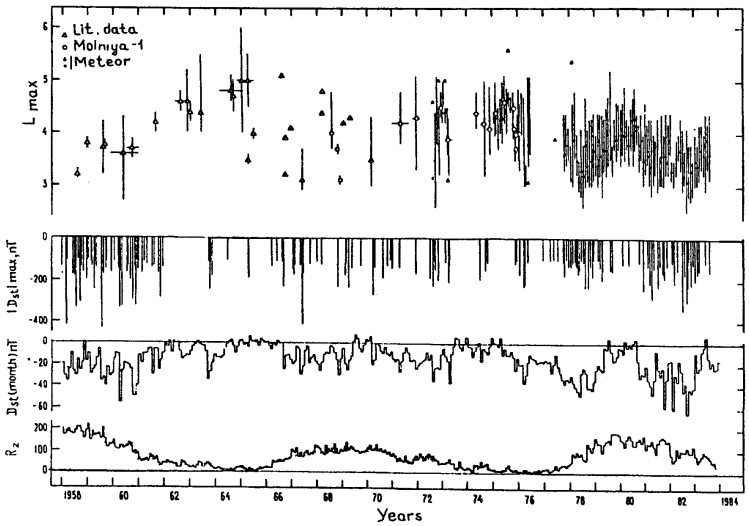

Fig.9. Outer radiation belt maximum position (Lmax) during the 1958-1984 time period (upper panel); storms with Dst >100 nT and monthly averaged Dst values (middle); sunspot numbers *W* (lower panel) (Tverskaya, 1996).

A relevant example of relativistic outer belt electron variations are long-term flux variations in geosynchronous orbit (at L~6.6). Fig.10 shows variations of electron fluxes with E_e>2 MeV and protons with E_p >2 MeV, measured on GOES during 1986-1997. It should be mentioned, that in general, the electron fluxes are poorly correlated with solar wind velocity increases, as it was assumed when the studies of these types of variations began. It is more probable, that there is a tendency towards flux increase at the decline phase of the solar activity cycle (1992-1996), than during its maximum (1990-91).

The physical mechanism of the above mentioned variations in outer zone electron fluxes is not yet clear. However, the existence of particle diffusion transport (see Fig.9) during geomagnetic activity increases should be regarded as the basis for a comprehensive physical description of this phenomenon. Even slight variations of the steeply declining electron spectra in the outer zone during amplification of the particle diffusion transport process inside the radiation belts can cause significant changes of the fluxes in the range of relativistic energies. These types of variations are not taken into account in any of the existing radiation belt electron models. Fig.11 illustrates the difference between the actually observed variations of ~1 MeV electrons measured on the GLONASS-94/1 satellite at L≈4.0, and AE-8 as well as RB/SINP model predictions (Panasyuk et al., 1996).

The radiation effects, induced by outer zone electrons are extremely important in onboard equipment radiation stability analysis. Primarily this concerns electric discharge processes deep in dielectric materials (see 3.3). According to CRRES data (Vampola et al., 1992), the deep dielectric discharges began when the currents reached ~ 0.1 pA/cm^2, which corresponds to electron fluences of 10^6 electrons/cm^2 (compared to the typical fluence values of 10^{12} electrons/cm^2 for electric discharge processes, obtained from ground data). The difference between estimates of the shielding thickness, required for preventing these processes, obtained using AE-8 and CRRES MAX models is quite striking: 300 mg/cm^2 and 750 mg/cm^2, respectively (Vampola, 1996). This clearly illustrates the ambiguity existing for the determination of the 'critical'

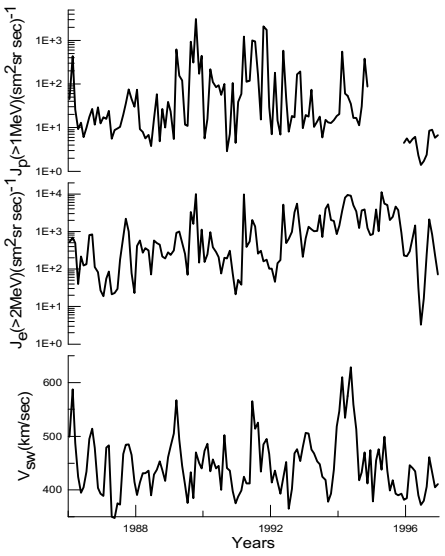

Fig.10. Variations of proton fluxes with E>1 MeV and electron fluxes with E>2 MeV (according to GOES satellite data) and solar wind velocity Vsw for the 1984-1996 time period (Dmitriev et al., 1999)

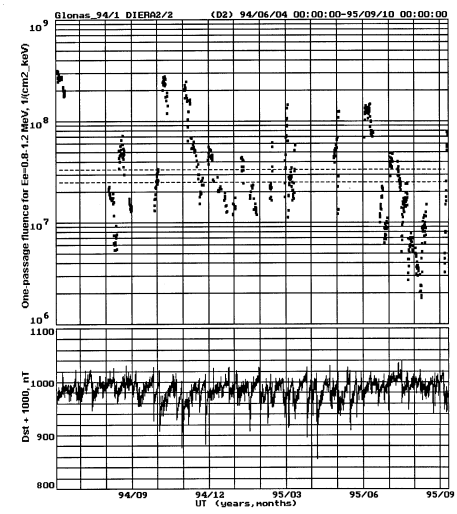

Fig.11. The 0.8-1.2 MeV electron flux as measured on the GLONASS-94/1 satellite. The data is represented in terms of fluence per passage through the belt. The corresponding model estimates are shownby the upper and lower dashed lines. The RB/SINP and AE-8 models were used. Dst index$_t$ is shown at the bottom. (Panasyuk, et al., 1997).

fluences inducing the electric discharge effect, and the surrounding radiation environment models. The existence of the rapidly varying outer zone electron fluxes leads to more significant long-term radiation dose variations in this region, than in the inner zone where the dose loads are mostly determined by the more stable high energy proton component (tens MeV and more). We present below the main types of variation for this inner zone component.

Inner Zone Protons. High energy protons of the inner zone are mainly generated by the albedo mechanism - decay of neutrons produced in interactions of primary GCR with the atmosphere. Due to weak variations of the source (GCR fluxes) and the slow processes of particle radial diffusion transport ($D_m \propto L^{10}$), the particle dynamics in this case is mainly driven by losses. For protons, these are mainly ionization deceleration in the upper atmosphere. Hence, the largest variation in the loss rate is observed near the outer edge of the radiation belts. Dose measurements made onboard orbital station 'Mir' during the last solar activity cycle show evidence of a significant solar cycle variation of the radiation in the SAA region (Fig.12).

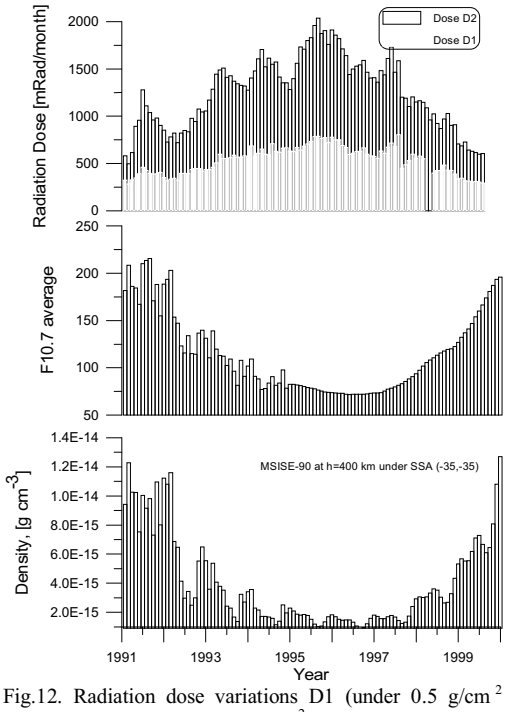

Fig.12. Radiation dose variations D1 (under 0.5 g/cm^2 shielding) and D2 (under 3.5 g/cm^2) onboard 'Mir' station during 1991-2000 as compared to the $F_{10.7}$ solar activity index and atmospheric density (according to the MSISE-90 model) at the altitude of 400 km (Bashkirov et al., 1998).

The radiation doses reach maximum values during solar cycle minimum, when atmospheric densities are minimum (the atmosphere gets cooler during periods of low solar activity). In other words, the minimum of the solar activity cycle corresponds to the maximum life-times of protons relatively to ionization losses (Bashkirov et al., 1998). Another process, which varies in 'phase' with the previous one, are GCR variations, the maximum of which is also reached during the minimum of the solar activity cycle. The amplitude of the variations for this component of the dose (D2), however, is significantly smaller (see the D2 variation in Fig.12), than for high-energy protons in the SAA region (D1). Fig.13 shows that the higher the satellite orbit, the smaller is the above mentioned solar-cycle variation effect (Huston et al., 1996).

The radiation doses, measured onboard 'Mir' station under 2 g/cm^2 of shielding during solar cycle minimum reached a relatively large value of 2000 mRad/month; this exceeds solar maximum values by a factor of 4-5. Such doses are a significant hazard for

prolonged missions since they substantially exceed the permitted limits for humans, accepted in many countries. Long-term radiation dose variations in the SAA region are driven not only by solar-cycle variations of atmospheric density, but also by secular variations of the Earth's magnetic field (see, e.g. (Bashkirov et al., 1998; Heynderickx et al., 1996). The angle of the geomagnetic dipole shifts by 6° in 20 years. This causes changes in the topology of the magnetic field especially in the SAA at low altitudes. As a result, the radiation intensity in this region increases with time, due to the associated secular decrease of geomagnetic field intensity. This secular variation of the multipole components of the geomagnetic field cause an increase of the L-shell parameter values in this region (over 40 years ΔL can reach 15%), simultaneously the longitude of the SAA shifts westwards. Though these changes are slow, they produce a significant change in the radiation flux at low altitudes, near the inner boundary of the radiation belts.

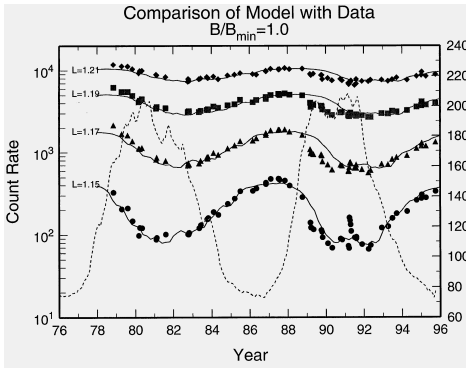

Fig.13. Variations of inner zone proton fluxes with energies E=80-215 MeV during 1976-1996 according to TIROS-NOAA satellite data as compared to the

As a consequence of its larger (51°) inclination the 'Mir' station orbit was more radiation hazardous (especially during years of solar activity minimum) than the standard 'Shuttle' orbit with a 28° inclination. For the future ISS, which has the same inclination as 'Mir', the radiation effects will, therefore, be similar. The ISS assembly will be carried out during the period of solar activity maximum in 2000-2002. During this time period the trapped radiation hazard will be minimum, however the SEP effect risk increases (see 4.5). The next increase of trapped radiation induced dose values can be expected during the next solar minimum (2004-2006).

Solar-cycle variations of high-energy radiation belt protons have been accounted for in the models based on the TIROS/NOAA data (Huston et al., 1996). These models adequately describe the radiation condition dynamics in LEO.

4.2. THE NEUTRON ENVIRONMENT

The neutron component in space has the following origin:
- solar neutrons, generated in the solar atmosphere as a result of nuclear reactions during active processes;
- albedo neutrons, which are a result of the interaction of primary GCR proton and SEP proton interactions with the atmosphere;
- local neutrons, generated in the satellite structure elements, as a result of GCR particle impact and energetic protons of the inner trapped radiation zone.

Neutrons, coming from the Sun, rarely reach the Earth's vicinity, since their half-decay time is short. The albedo neutron fluxes at low altitudes increase with latitude in concordance with the well-known Lingenfelter dependence, which reflects the GCR latitude effect. This dependence is in good agreement with the data of different experiments (see e.g. (Lockwood, 1973)).

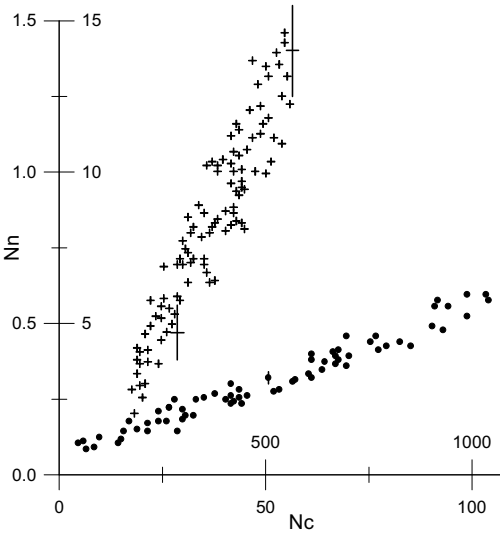

Fig.14. Neutron count rate (Nn) versus charged particle count rate (Nc, both in s^{-1}) in the SAA (solid circles, upper and right scales on the axes) and outside the SAA (crosses, lower and left scales on axes) according to 'Salyut-6' station data. (Yushkov, 1988).

The local neutron flux depends on both the primary particle spectra and spacecraft mass. The first effect can be illustrated by Fig.14, obtained using 'Saluyt-6' data (Yushkov, 1988) : outside the SAA the efficiency of local neutron generation is greater than inside the SAA, where the spectrum of trapped protons is softer. The dependence of neutron generation on the mass of the spacecraft is illustrated in Fig.15. With increasing satellite mass, the local neutron flux increases (Bogomolov et al., 1998). An increase of the shielding thickness of the satellites leads to an increase of the neutron component radiation doses. Thus, according to direct measurements on 'Mir' station, the radiation dose under several tens of g/cm^2 shielding is mainly induced by neutrons (see Table 2.)

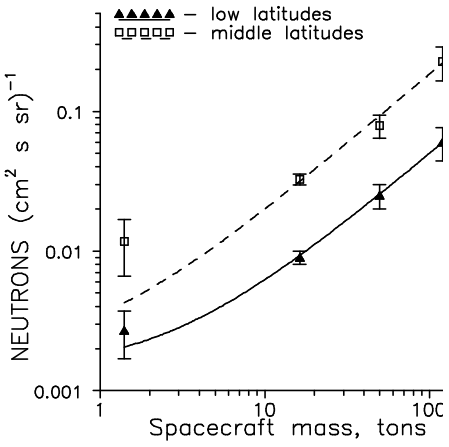

Fig.15. Mass dependence of neutron fluxes at low and

Besides the dose effects, induced by the neutron component, local and albedo neutrons can cause single event upset effects in onboard electronics. This effect is associated with products of nuclear reactions, occurring in the satellite materials. It is assumed that SEU induced by background neutrons have production cross-sections comparable with proton SEUs, but with lower energy threshold (Pickel, 1996).

TABLE 2. Ionizing radiation doses (D_i) and corresponding neutron induced radiation doses (D_n) under different shielding thicknesses, measured on 'Mir' station (Lyagushin et al., 1997) during solar activity maximum (1990-93).

Shielding g/cm^2	Dose μSv/day	
	D_i	D_n
20	143	76
30	92	115

4.3. GALACTIC COSMIC RAYS

4.3.1. *Empirical Models*

Cosmic rays of galactic origin with energies below several hundred GeV are subjected to solar modulation: with increasing/decreasing solar activity the GCR fluxes decrease/increase. The quantitative description of these variations is built in the various GCR models. At present the GCR model developed at SINP MSU most completely describes the dynamics of all the GCR components ($1 \leq Z \leq 92$) in a wide range of energies E=1- 10^5 MeV/nucleon (Nymmik et al., 1995). The GCR/SINP models provide a more adequate description of the behavior of the main nuclear components as well as electrons, than the widely used CREME model (Adams, 1985). The inter-comparison of these models (Nymmik et al, 1995) is given in Fig.16. The typical errors do not exceed 20%. The dynamic GCR/SINP model establishes a direct connection between the particle fluxes and solar activity (the Wolf number - W). The time lag for the particle arrival in Earth orbit has been accounted for. The basic concepts of this model are the following:

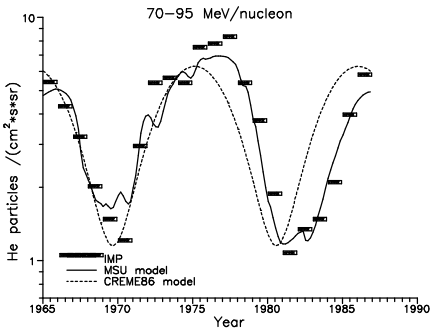

Fig.16. Comparison of GCR/SINP (solid line) and CREME (1986) (dashed line) models with 70 MeV<E<95 MeV helium experimental data (IMP-8) according to (Nymmik et al., 1995).

(a) the angular distribution of GCR particle fluxes at the Earth orbit outside the magnetosphere is assumed to be isotropic;
(b) the solar activity level is described by the 12 month smoothed value of $\overline{W}$;
(c) variations of the large-scale magnetic fields in the heliosphere are assumed to be proportional to the variations of the magnetic field of the Sun, which depends on the level of solar activity and the characteristics of its cycles (odd or even);

(d) the dynamics of large-scale GCR modulations are characterized by the modulation of the effective electric potential of the heliosphere $R_0(R,t)$, which is a function of $\overline{W}$, of time, of the time lag between GCR flux variations and solar activity variations (which in turn depend on particle rigidity R), the phase of the solar activity cycle t in the odd and even cycles.
(e) the differential spectra of GCR fluxes as a function of energy and rigidity are defined according to an empirical technique based on experimental data.

Currently the GCR/SINP model is incorporated into the CREME-96 model, developed in the USA (Tylka et al, 1997).

4.3.2. *GCR Induced Radiation Effects*

As it was already mentioned in section 2, the main radiation effect induced by GCR are single event upsets (SEU) in the memory chips of onboard electronic systems. Therefore it is interesting to compare the results of SEU model calculations and the corresponding experimental data. Currently a vast number of papers are available (see e.g. (Bendel and Petersen, 1983; Campbell et al., 1992), which contain data on SEU rates in various types of memory chips, obtained in actual space flights. These data, apart from direct verification of the sensitivity of various microchips to SEU occurrence in flight conditions, provide the opportunity for verification of the SEE and radiation belt environment models.

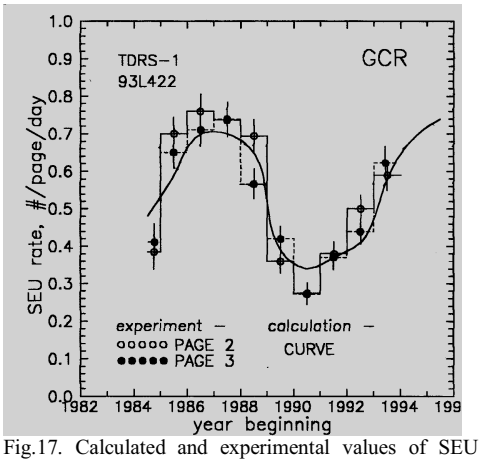

Fig.17. Calculated and experimental values of SEU rates in geostationary orbit (the TDRS satellite) (Adams et al., 1996). PAGE 2 is the working chip , PAGE 3 is the backup chip.

Among the numerous data on SEE, acquired in space, the TDRS-1 geostationary satellite data are very important, since they cover a large part of the 22-year solar activity cycle. Fig.17 shows simulated and experimental SEU rate values in the Fairchild 93 L422 microchip, without taking into account the large SEP events, which can also cause SEU (Adams et al., 1996). The simulated values of SEU rates were obtained using the GCR/SINP model, described above. They take into account for the distribution of shielding matter surrounding the chip. The conducted study reaches an optimistic conclusion about the capabilities of this model to predict GCR induced SEE effects.

4.4. ANOMALOUS COSMIC RAYS

It was already mentioned in section 2.3 that ACR can penetrate inside the Earth's magnetic field and undergo charge exchange in dense layers of the atmosphere, forming

a shell of multicharged ions. The maximum particle intensity of this belt at L≈2÷2.5, exceeds by a factor of several hundreds the intensities of corresponding ion fluxes outside the magnetosphere (Grigorov et al., 1991; Selesnik et al., 1996). The temporal variations of the trapped ACR component are similar to interplanetary ACR flux variations, which, apparently, can be explained by the short life-times of trapped ACR (Grigorov et al., 1991). Therefore, the maximum fluxes of trapped ACR particles, are observed during maximum of the solar activity cycle. An analysis of the experimental data of the 'Cosmos' and 'SAMPEX' satellites was made in (Tylka et al., 1997) in order to calculate the LET spectra of trapped ACR for typical LEO orbits and their comparison of LET spectra for GCR and extra-magnetospheric ACR. The results of the analysis show that ACR cannot play a significant role in SEU generation, except for very thin shielding and small inclination low altitude orbits where their contribution becomes predominant.

4.5. SOLAR ENERGETIC PARTICLES

4.5.1. *Empirical models*

Modern solar physics is not capable of predicting SEP generation, and, thus not their dependence on solar activity. Therefore the probabilistic models of SEP events have been designed. In order to build such models is it is necessary to find the regularities in the occurrence rates of SEP events. It has been found that they depend on the following parameters:

- time;
- fluence and peak flux magnitude;
- elemental ion and isotopic composition;
- particle energy.

Most of the models developed so far are not capable of describing all these characteristics together. They are restricted to extreme cases, and, as a rule, provide only the proton flux. Hence, in the CREME (Adams, 1985) model, all the SEP events are reduced to 'ordinary', 'worst case' and 'anomalously large' types. In this model, the proton energy spectra for the first two types of events are represented by the sum of two exponential functions of energy, and the 'anomalously large' event is described by the extreme SEP of August 1972 (and subsequently by the mean of the August 1992 and February 1956 events). The CREME 96 version of the model (Tylka et al., 1997) uses the October 1998 event as the 99% 'worst case'. The probability of an event occurrence during years of solar activity maximum is described by the Burrell statistical model.

The heavy ion energy spectra are separated in to two different classes - the 'ordinary' and 'heavy ion enriched' events. It is assumed, that the ratios between heavy ion fluxes in SEP events do not depend on the energy of the particles. Other models (see, e.g. (Feynman, et al., 1992)) consider only the probabilities of the occurrence of SEP events of different fluences, and do not account for the existence of heavy ions in SEP events.

The recently developed SEP/SINP (Nymmik, 1999) model describes the characteristics of both fluences and peak fluxes of the solar event proton and ion events. Whereas in all the previous models it was assumed, that the probability of a SEP event over several years of active Sun is the same as over other phases of solar activity, the

SEP/SINP model is based on the concept, that the mean occurence frequency of proton fluences is indeed a function of solar activity. Thus, the mean occurrence frequency (events per year) of SEP events $\overline{\nu}$ with fluences $\geq 10^5$ protons/cm^2 is defined by the power law:

$$\overline{\nu}(t) = 0.3 \cdot \overline{W}(t)^{0.75}, \quad (4)$$

where $\overline{W}$ are Wolf numbers avaraged over 12 months. The distribution of $\overline{\nu}$ as a function of fluence, as well as the differential energy spectra of both fluences and the peak flux values (for all the particles in the $E \geq$ 30 MeV/nucl) are also power law functions in this model (see Fig. 18). These functional regularities were established on the basis of experimental data. The power law dependence, as opposed to the log-normal one, is the main difference between the SEP/SINP model and all other earlier alternative models. The probabilistic SEP/SINP model enables to calculate the energy spectra of all the main SEP components for any space mission duration ranging from 1 month to 11 years and to provide event probabilities.

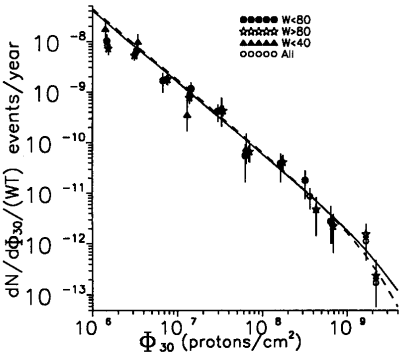

Fig.18. Distribution of solar events in proton fluences for different solar activity periods. (The corresponding sunspot number values - W are shown in the upper part of the figure) (Nymmik, 1999).

4.5.2. *SEP Induced Radiation Effects*

Fig.19 shows the energy dependence of the SEP fluence energy dependence calculations (the solid lines are differential energy, the dashed lines are integral spectra) for the whole 22-nd cycle (left) and solar activity minimum periods (limited to four 4-year intervals around solar minimum). GCR calculations, employing the GCR/SINP model for the corresponding time intervals are also shown. It should be noted, that even during periods of the quiet Sun, the differential fluences of SEP protons exceed GCR fluences (for energies up to ~ 100 MeV). This result demonstrates how important it is to account for SEP when estimating the total radiation effect.

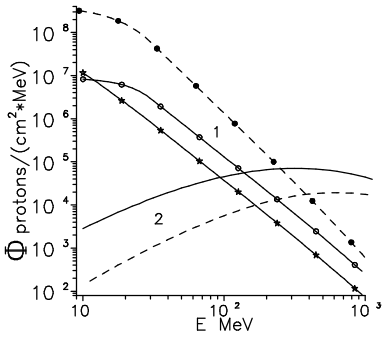

Fig. 19. The differential energy spectra of annual proton fluences according to the model (Nymmik, 1999) for 'quiet' Sun periods (open circles) and time periods close to maximum (dark circles). The solid and dashed lines (1) are experimental data extrapolations to high energies for 'quiet' Sun and high solar activity, respectively. The solid and dashed lines (2) are the annual integral galactic proton spectra for the same solar activity levels.

Nevertheless, it is necessary to emphasize, that additional research is needed to verify the basic results of the SEP/SINP model and other models to achieve an adequate and more definitive description of the radiation effects with respect to SEP events.

Another important problem of SEP modeling is to determine their characteristics after penetration inside the magnetosphere. This stage of modeling implies knowledge of the cut-off rigidity values. In this case the particle fluxes depend on the geographical coordinates of the altitude, latitude, longitude of the point of observation in the magnetosphere on the particle energy E, and on its direction of arrival.

Our understanding of the cutoff rigidity has significantly changed over the past years. The transition from the first calculations using the dipole model of the terrestrial geomagnetic field (the Stormer approximation) to the multi-pole IGRF fields, accounting for various current systems inside the magnetosphere and on its surface, contributed to our current level of understanding of the rigidity cutoff. Therefore, the calculations, concerning SEP penetration inside the magnetosphere, require the use of dynamic magnetic field models, which account for geomagnetic disturbances. The widely used Tsyganenko model (Tsyganenko, 1989) satisfies these requirements.

An example of calculated penetration functions for ISS orbit depending on geomagnetic cutoff for different levels of geomagnetic activity is given in Fig.20. The calculations were made using the technique suggested in (Danilova and Tyasto, 1995), which provides penetration function calculations with an accuracy better than 10%. It can be seen that the SEP particle flux in the low-energy part of the spectrum (<100 MeV) strongly depends the level of geomagnetic activity. In reality, even in very low orbits (such as piloted orbital station orbits), the penetration of SEP, is the main radiation hazard factor during powerful events on the Sun, accompanied by magnetic storms. Thus, during the solar events of October 19th 1989 and March 24th, 1991, the integral radiation doses on 'Mir' station (induced by SEP penetration) increased by large factors of 2.5÷3 during several hours (Aristova et al., 1991). It should be noted, that up to shielding thicknesses of several g/cm^2 the SEP radiation doses exceed the estimated dose values induced by both GCR and trapped radiation belt protons and electrons during these extreme SEP events.

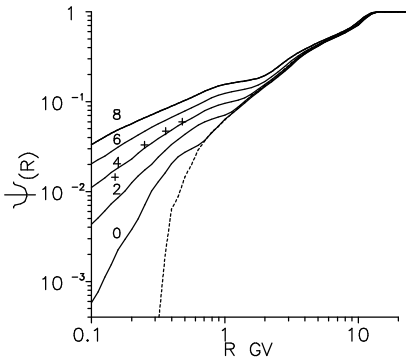

Fig.20. Penetration function (Ψ) for SEP depending on rigidity (R) for an ISS orbit at different Kp-index values. The crosses are modeling results (Aristova et al., 1991) for Kp=5.

Besides dose effects, protons and other SEP ions can cause SEU. Table 3 shows the experimental and calculated data of the total SEU number (over the whole SEP event) for large SEP events in 1989-1991. The experimental data are represented by the averaged annual values for control unit microchips (93L422) of the TDRS-1

geostationary satellite. The calculation was made by taking into account of the distribution of shielding matter, surrounding the microchips.

It is obvious that the calculated SEU rate under SEP impact is formed in approximately equal proportions by protons and ions, which is a consequence of the distribution of shielding matter around the chip. Comparison of the experimental and calculated values shows that the average discrepancy between them is ±60%, and in the worst cases it reaches a factor of ~2.5. These discrepancies are probably explained by the difference between the actual SEP spectrum and the 'mean event' spectrum used in the model.

TABLE 3. Experimental and calculated values of the total number of SEU on the TDRS-1 satellite (Adams et al., 1996).

SEP event	Experimental value	Calculated values		
		Protons	Ions	Total
August 1989	10±3	15	9	24
September 1989	34±6	21	17	38
October 1989	98±10	70	57	127
March 1991	8±3	8	7	15
May 1991	24±5	10	10	20

4.6. THE NEAR-EARTH 'INTEGRAL' RADIATION ENVIRONMENT

The radiation impact of the space environment, surrounding the Earth, is formed by a combination of individual components, such as: radiation belts, albedo particles, galactic and solar cosmic rays. The actual impact of each of these factors is to a large extent determined by the orbit of the satellite, its construction (shielding of individual units and the volume of the modules), and the time of the satellites active existence in near-Earth space. The flight is conducted in different space radiation fields, with essentially different space-time characteristics.

Therefore, radiation effect characteristics should account for two cases - the maximum, peak particle flux and the averaged (daily mean, annual mean, etc.) flux, which should be recorded in orbit during prolonged missions. The first case permits to estimate the spacecraft 'survival' in extreme conditions, the second one - the overall level of serviceability. We will discuss the specific features of 'integral' radiation effects using several typical satellite orbit as an example.

4.6.1. *Low Earth Orbit*

The term LEO is usually used in reference to orbits with perigee altitudes below 1000 km. All piloted spacecraft, spacecraft performing Earth surface observations, etc., typically operate at these altitudes. The radiation belt particle fluxes in these orbits are

extremely time-dependent, and vary significantly for certain orbit revolutions ranging from minimum (zero for empirical RB models) levels to maximum ones (exceeding the average level by orders of magnitude) during flight intervals of several minutes. The maximum RB particle flux values are observed in the SAA region, therefore 'peak' flux values should be calculated for orbit revolutions, passing over the center of the SAA.

The mean RB particle fluxes are calculated as a result of model flux averaging for one day of the flight, during which some of the orbits pass over the SAA center. It should be mentioned, that satellites in LEO orbit spend most of the mission time at altitudes, where the particle drift shells are not distorted by geomagnetic disturbances, therefore, the calculations, are, as a rule, made for a quiet geomagnetic field. GCR particles and SEP are subject to complex time variations in LEO. First of all, these are their own variations in the interplanetary medium; secondly, these are variations associated with GCR and SEP particle penetration into different parts of the orbit under different geomagnetic activity conditions. Satellites with sufficiently large orbit inclinations at high altitudes, enter regions where GCR and SEP fluxes are predominant.

When making GCR flux impact predictions it is reasonable to use their flux calculations for the epoch of solar minimum, when maximum fluxes of these particles are observed. When calculating SEP fluxes, it is necessary to account for the probabilistic nature of SEP event occurrence. Therefore, the maximum estimated SEP flux, should be found according to the peak flux of an event, which is expected with a certain probability. The mean daily flux has to be substituted by the 'mean' flux value, achieved in one event with the same probability over a long (not less than 11 years) time period. The maximum estimated SEP flux should be calculated for interplanetary medium conditions, and the mean flux estimates should take into account the particle penetration function into a given orbit.

Fig.21 shows the results of annual radiation dose predictions for the ISS orbit. The calculations were made (Kuznetsov and Lobakov, 1999), using the generalized model of SEU calculations, described in (Bendel et al., 1983) and the SEP/SINP model (Nymmik, 1999), the GCR/SINP (Nymmik et al., 1995), and AP8 (Sawyer and Vette, 1979). The conclusions, concerning ISS operation, which can be made from the calculations presented above, are the following:

1) The radiation doses are mainly induced by RB particles (protons), in the whole range of reasonable shielding thicknesses. During minimum solar activity the radiation doses are maximum.

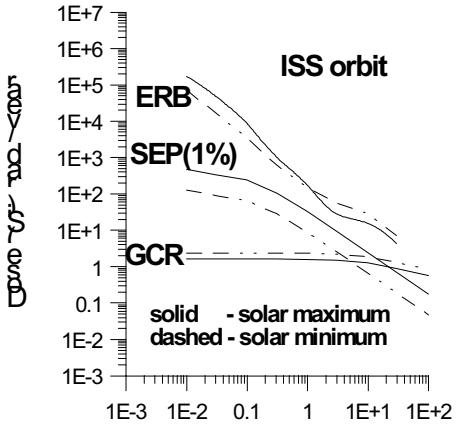

Fig.21. The radiation doses in ISS orbit under different shielding thicknesses, calculated using RB/SINP, GCR/SINP and SEP/SINP models for an 11-year period of active existence (Kuznetsov and Lobakov,

2) The largest SEU rates should be expected for very large SEP events, which occur with a 1% probability. Most of the SEP events give significantly lower SEU rate levels. For example, 50% of the SEP lead to SEU with rates, significantly lower, than the rates of GCR induced SEUs.
3) Simultaneously, it can be noted, that under the impact of only one of the radiation components GCR or SEP, for small thickness of spherical shielding, the SEU rate grows with increasing shielding thicknesses. This effect is most pronounced for SEP particles.

4.6.2. *Geostationary Earth Orbits - GEO*

This type of orbit is characterized by the existence of rapid variations of RB particle fluxes (see 2.1.) as well as SEP and GCR variations, typical for interplanetary space. Examples of SEU calculations under the impact of GCR and SEP in geostationary orbit are given in 4.3.2 and 4.5.2. respectively. The peculiarities of dose effect calculations are given in 3.3. It is necessary to mention, that the existence of rapid variations of the electron component in the outer RB region on time scales from fractions of a minute to several days during geomagnetic storms, as well as solar cycle variations, makes it difficult to use RB models (which are essentially static) for precise calculations of the radiation load.

4.6.3. *High-apogee Elliptic Orbits - HEO*

Such orbits (with perigee and apogee altitudes from several hundred to several thousand kilometers) typically intersect both the inner and outer RB zones. Therefore, SEU calculations besides cosmic ray particle fluxes should account for the impact of trapped protons of the inner zone. Fig.22 shows the SEU rate calculations in microchips on the CRRES satellite, depending on the L-shell parameter for inner RB zone protons and GCR particles (for shielding thicknesses of 10g/cm^2) (Bashkirov et al., 1999). The observed experimental data on L<2 can be adequately described by the impact of RB protons. The maximum number of upsets is observed in the range of L-shells, where the satellite encounters the maximum proton flux on L~1.5 (for orbit altitudes of ~2500-3000 km). However, the results of GCR induced SEU calculations in the outer zone do not coincide with the experimental results, which requires additional analysis.

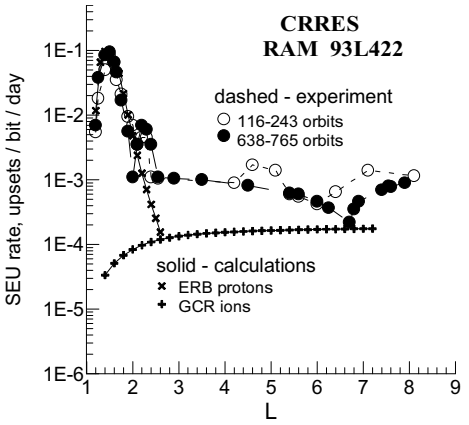

Fig. 22. Experimental results from CRRES and SEU rate calculations according to the model (Bashkirov et al., 1999).

5. Conclusions

Existing trapped radiation models can only be used as indicative ones. For more accurate model calculations of the radiation environment it is necessary to use available experimental data for specific orbits and time periods.

Our current understanding of the types of particle variations in the RB already permits to make estimates of the particle fluxes on time scales ranging from substorms to the whole solar cycle.

The existing dynamic GCR model (GCR/MSU, CREME 96) adequately describes the variations of GCR nuclei and can be utilized for accurate radiation effect calculations.
The solar energetic particle model which is essential for engineering calculations of radiation effects has not yet been completed. There are significant discrepancies between the new Solar Energetic Particle model developed at MSU (SEP/SINP) and previous models (CREME 96, JPL 91, etc.).

The albedo environment in LEO requires systematization, and, possibly additional physical modeling aimed at developing a comprehensive albedo radiation model, incorporating all the radiation components at low altitudes.The accuracy of secondary particle flux models depends on both the accuracy of the specific spacecraft shielding and mass distribution, and on the surrounding environment model. Utilization of modern transport codes like GEANT is required for modeling the radiation environment inside the spacecraft.

The high level of integration and miniaturization of modern electronics is the most 'sensitive' aspect of our current understanding of radiation effects on space systems. New electronics demands not only improved accuracy of radiation environment models and calculations, but also more accurate studies of the physical mechanisms of charged particle interactions with the spacecrafts material.

While accomplishing space experiments we need to keep in mind, that the space environment is aggressive towards any man-made object placed inside it, including towards man himself. There are no orbits or time intervals which would be completely radiation-safe. The question is how hazardous these effects of the aggressive environment can be, what are the most suitable and acceptable radiation thresholds to be proposed as optimized international standards.

Acknowledgements

The author sincerely wishes to thank the organizers of the NATO Advanced Study Institute on Space Storms and Space Weather Hazard - the Directors of ASI Dr. Ioannis Daglis and Prof. Yurii Galperin for the opportunity to present this tutorial lecture and to publish it in these proceedings. The author is extremely grateful to Prof. Joseph Lemaire for many valuable comments.

References

Adams, J. (1985) Cosmic ray effects on microelectronics, in *Naval Research Laboratory Memorandum Report,* **IV**, Washington, USA, 1- 118.

Adams, J., Belyaev A.A., Kuznetsov, N.V. and Nymmik, R.A. (1996) Occurrence frequency of single upsets induced on synchronous orbit: model and calculations with TDRS–1 experiment, *Nuclear Tracks & Radiation Measurements* **22,** 509- 512.

Akishin, A.I., Aleksandrov, A.P. (1983) Imitation testing space material science, in S.N.Vernov (ed), *Space model* (in Russian), Moscow State University Publishers, Moscow, **2**, 9-28.

AMS collaboration, Protons in near earth orbit, *Phys. Letters*, (2000), **B472,** 215 – 225.

Aristova, I.N., Lyuagushin, V.I., Marin, B.V., Saraeva, M.A., Tel'tsov, M.V. (1991) Radiation environment on the orbital complex MIR during September- October 1989, *Kosmicheskie Issledovaniya,* **30**, 794-798. (in Russian).

Baker, D.N. (1996) Solar wind-magnetosphere drivers of space weather, *J. of Atmospheric and Terrestrial Physics,* **58**, 1509-1526.

Bashkirov,V.F., Panasyuk,M.I., Teltsov, M.V. (1998) Trapped radiation dynamical model for low altitudes in the magnetosphere, *Kosmicheskie issledovaniya* (in Russian) **36,** 359-368.

Bashkirov, V.F., Kuznetsov N.V., Nymmik, R.A., (1999) An analysis of the SEU rate of microcircuits exposed by the various components of space radiation, *Radiation. Measurements*., 30 (1999), 427- 433.

Beliaev, A.A., Lemaire. J., (1994) Evaluation of the INP radiation belt models, TREND Technical note A, ESTEC contract no. 9828/92/NL/FM.

Beliaev, A.A., Lemaire J., (1996) Comparison between NASA and INP/MSU Radiation belt models, in J.Lemaire, D. Heynderickx, D. Baker, (eds.), *Radiation belts: models and standards,* Geophysical Monograph **97**, 141-145.

Bendel, W. L., Petersen E.L. (1983) Proton upsets in orbit, *IEEE Trans. on Nuclear Science* **NS- 30,** 4481- 4485.

Binder, D., Smith, E.C., and Holman, A.B. (1975) satellite anomalies from galactic cosmic rays, *IEEE Trans. on Nucl. Sci.* **22,** 2675-2680.

Blake, J.B., Friesen, L.M. (1977) A technique to determine the charge state of anomalous low energy cosmic rays, *Proc. 15th Int. Cosmic Ray Conference.,* **2**, 341-346.

Bogomolov, A.V., Bucik, R., Dement'ev, A.V., Denisov, Yu.I., Ryumin, S.P. (1998) Energetic neutron and gamma ray spectra under the earth radiation belts according to fluxes observed onboard Coronas-I satellite, Salut-7- Cosmos -1686 orbital complex, *Adv. Space res.,* **21**, 1801-1804.

Brautigam, D.H., Gussenhoven, M.S.,Mullen, E.G. (1992) Quasistatic model of outer zone electrons, *IEEE Trans. Nucl.Sci.,* **39**, 1797-1809.

Campbell, A., McDonald, P., Ray, K. (1992) Single event upset rates in space, *IEEE Trans. on Nucl. Sci*. **39**, 1828-1835.

Danilova, O.A., and Tyasto, M.I. (1995) Cosmic ray cutoff rigidities in the Tsyganenko's magnetospheric magnetic field models of 1989 and 1987 years, *Proceeding 24th Int. Cosmic Ray Conference, Roma* **5,** 1066- 1069.

Desorger, L., Buhler, P., Zehnder,P., Daly, E., Adams,L.(1998) Outer radiation belt variations during 1995, *Adv. Space Res.,* **22**, 83-87.

Dmitriev A.V., Kalinin D.V., Kuznetsov S.N., Yushkov B.Yu. (1999) "Variations of the geomagnetic indices that control the radial diffusion of energetic particles in radiation belts".*Proceeding of Space Radiation Environment Workshop (SREW)*, Farnborough, England. 1-3 Nov, 1999 (in print).

Ebert, W.L., Hoffman, E.J. (1999) Quality and reliability: APL's key to mission success, *John Hopkins APL Technical Digest,* **20,** 496-506.
Feynman J., Spitale, G., Wang, J., and Gabriel, S. (1992) Interplanetary proton fluence model, *J. Geophysical Research***, 98**, 1328-1342.
GEANT (3.16 , 3.21) Detector Description and Simulation Tool, CERN Geneva, Switzerland, 1994.
Gloeckler G. (1979) Galactic cosmic ray, *Rev.Geophys. and Space Phys*, **17,** 569-582.
GOST 25645.138-86, GOST 25645.139-86 (1986) The natural radiation belts , *Standart Publishers* (in Russian).
Grigorov, N.L. (1985) *High energy electrons in the vicinity of the Earth,* Nauka Academic Publishers, Moscow (in Russian).
Grigorov,N.L., Kondrat'eva, M.I., Panasyuk,M.I., Tretyakova, Ch.A., Adams J., Blake, J.B., Schulz, M., Mewaldt, R.A., Tylka, A.(1991) An evidence for anomalous cosmic ray oxygen ions in the inner magnetosphere, *Geophys. Res. Lett.,* **18**, 1959-1962.
Gussenhoven, M.S., Mullen, E.G., Sperry, M., Kerns, K.J. (1992) The effect of the march 1991 storm on accumulated dose for selected orbits: CRRES dose models, *IEEE Trans. Nucl. Sci.,* **39**, 1765-1778.
Heynderickx, D., Kruglanski, Lemaire, J.F., Daly, E.L. (1996), in J.Lemaire, D. Heynderickx, D. Baker, (eds.), *Radiation belts: models and standards,* Geophysical Monograph ,**97**, Washington, 173-178.
Huston, S.L., Kuck, G.A., Pfitzer, K.A. (1996) Low- altitude trapped radiation model using TIROS/NOAA data, in J.Lemaire, D.Heynderickx, D.Baker (eds.), *Radiation belts: models and standards,* Geophysical Monograph, **97**, Washington, 119-128.
Ilyin, V.D., Kuznetsov, S.N., Panasyuk, M.I. , and Sosnovets, E.N. (1988) Nonadiabatic effects and limit of proton capture in the Earth's radiation belts*, Bull. Acad. Sci. USSR, Phys. Ser. (USA) ,***48**, 134-137.
Kuznetsov N.V., Lobakov A.P.(1999) *An estimate of dose and single event effects on low-Earth orbit spacecraft.* In: Space Radiation Environment Workshop & Workshop on Radiation Monitiring for the International Space Station. Book of Abstracts, 51.
Kuznetsov, N.V., Nymmik, R.A. (1994) Background ion fluxes as a source of single events effects of microelectronics onboard spacecrafts, *Kosmicheskie issledovaniya* (in Russian) **32**,112-117.
Kuznetsov, S.N., Myagkova, I.N., Yushkov, B.Yu. (1999) Connection between Energetic particle Fluxes at Geostationary orbit with solar wind parameters and with solar cosmic rays*. Proceeding of Space Radiation Environment Workshop SREW),* Farnborough,England. 1-3 Nov.1999 (in print).
Lemaire, J., Johnstone, A.D., Heynderickx, D., Rodgers, D., Szita, S., Pierrard, V., Trapped Radiation Environment Model Development: TREND-2, Final Report, Aeronomica Acta A-393, 1995.
Lockwood, J.A. (1973) Neutron measurements in space, *Space Science Rev.,* **14**, 663-675.
Lyagushin, V.I., Sevastyanov, V.D., V.D., Tarnovsky,G.V. (1997) A measurements of energetic spectrum of neutrons on orbital station "Mir", *Kosmicheskie Issledovaniya*, **35**, 216-225 (in Russian).

Makletsov, A.A., Mileev, V.N., Novikov, L.S., Sinolits, V.V. (1997) Radiation environment modeling onboard spacecrafts, *Engineering Ecology,* **1,** 39-51 (in Russian).

McIlwain, C.E. (1996) Processes Acting upon outer zone electrons, in 'Radiation belts: Models and Standards', in J.Lemaire, D.Heynderickx, D.Baker (eds.), *Radiation belts: models and standards,* Geophysical Monograph 97, Washington.

Morfill, G.E.(1973) Guiding center approximation of trapped particles, *J. Geophysical Research,* **78***,* 588-593.

Nymmik R.A.(1999) Probabilistic Model for fluences and peak fluxes of solar energetic particles", *Radiation measurements*, **39**, 287-296.

Nymmik,R.A., Panasyuk, M.I., and Suslov, A.A. (1995) Galactic cosmic ray flux simulation and prediction, *Adv. Space Res.* **17**, 19-23.

Ormes, J.F., Betty, J., Binns W., Wiedenbeck, M. (1994) Galactic Cosmic Rays upto 10 TeV, in "Particle and Nuclear Astrophysics and Cosmology in the Next Millenium". *Proceedings of the 1994 Snowmass Summer Study*, edited by . E.W. Kolb and R.D. Pecei, 312-323.

Panasyuk, M. I. (1993) Anomalous cosmic ray studies on "Cosmos" satellites, *Proc. 23th Int. Cosmic Ray Conference,* **4**, 455-463.

Panasyuk, M.I., Sosnovets,E.N., Grafodatsky,O.S., Verkhoturov,V.I., Islyaev,Sh.N. (1996) First results and perspectives of monitoring radiation belts, in J.Lemaire, D.Heynderickx, D.Baker (eds.), *Radiation belts: models and standards,* Geophysical Monograph 97, Washington, 211-216.

Pickel, J.C. (1996) Single event effect prediction, *IEEE Trans. Nucl. Sci.* **43**, 483-495.

Rodgers, D.J., (1996) A New Empirical Electron Model, , in 'Radiation belts: Models and Standards', in J.Lemaire, D.Heynderickx, D.Baker (eds.), *Radiation belts: models and standards,* Geophysical Monograph , **97**, Washington,103-107.

Sawyer, D.M., Vette, J.I. (1979) AP-8 trapped proton environment for solar maximum and solar minimum, *NSSSDC/WDC-R&S.*

Selesnik, R.S., Cummings, J.R., Mewaldt, R.A. (1996) Observations of geomagnetically trapped anomalous cosmic rays by SAMPEX, in Reeves,G.D.(ed), *Workshop on the Earth's trapped particle environment,AIP Conference Proceedings,* **383**, 155-160.

Seltser, S.M. (1979) Electron, electron-bremsstrahlung and proton depth-dose data for space shielding applications, *IEEE Trans. Nucl. Sci.,* **NS26**, 21-60.

Spejeldvik, W.N.(1979) Transport,charge exchange and loss of energetic heavy ions in the Earth's radiation belts: applicability and limitation of theory, *Planetary Space Sciences,* **20**, 1215-1226.

Tsyganenko, N.N. (1989) A magnetospheric magnetic field model with a wrapped tail current sheet, *Planetary Space Sciences* **37**, 5-20.

Tverskaya, L.V. (1996) Dynamics of energetic electrons in the radiation belts, in J.Lemaire, D.Heynderickx, D.Baker (eds.), *Radiation belts: models and standards,* Geophysical Monograph **97**, Washington, 183-187.

Tverskoy, B.A.(1964) Dynamics of radiation belts, *Geomgnetizm i aeronomiya,* **5**, 436-441 (in Russian).

Tylka, A., Adams, J., Boberg, P.R., Brownstein, B., Dietrich, W.F., Fluechiger, E.O., Petersen, E.L., Shea, M.A., Smart D.F., and Smith, E.C. (1997) *CREME96: A revision*

of the cosmic ray effects on microelectronics code, IEEE Transactions on Nuclear Science, **44**, 2150- 2160.
Vakulov, P.V., Kovrigina, L.M., Mineev, Yu.V., Tverskaya, L.V. (1976) Variations of intensity and spectrum of energetic electrons in the earth of radiation belts during strong magnetic disturbances, *Space Res.,***16**, 529-532.
Vampola, A.L., Osborn, J.V., Johnson, B.M. (1992) The CRRES magnetic electron spectrometer AFGL 701-5A (MEA), *J. Spacecraft & Rockets,* **29**, 592-594.
Vampola, A.L., (1994) Analysis of environmentally induced spacecraft anomalies, *J. Spacecraft & Rockets*, **31**, 154-159.
Vampola, A.L. (1996) The nature of bulk charging and its mitigation in spacecraft design, *In WESCON Proc,* Anaheim, California, 234-241.
Vette, J.I. (1991) The AE-8 trapped electron environment, *NSSSDC/WDC-R&S.*
Williams, D.J., Arens, I.F., Lanzerrotti, L.T. (1968) Observations of trapped electrons at low and high altitudes, *J. Geophys. Res.* **73**, 5673-5689.
Williams,D. (1966) 27-day periodicity of the trapped electron fluxes, *J.Geophys. Res.,* **71**, 7-21.
Yushkov., B.Yu., (1988), Neutron flux measurements onboard Salyut-6 orbital station, *Kosmicheskie issledovaniya*, **26**, 793-796 (in Russian).